ANTIOXIDANTS & REDOX SIGNALING
Volume 21, Number 12, 2014

DOI: 10.1089/ars.2013.5597

ORIGINAL RESEARCH COMMUNICATION

Concomitant Inactivation of *Foxo3a* and *Fancc* or *Fancd2* Reveals a Two-Tier Protection from Oxidative Stress-Induced Hydrocephalus

Xiaoli Li,[1] Liang Li,[1] Jie Li,[2] Jared Sipple,[1] Jonathan Schick,[1] Parinda A. Mehta,[3,4] Stella M. Davies,[3,4] Biplab Dasgupta,[1,4] Ronald R. Waclaw,[1,4] and Qishen Pang[1,4]

Abstract

Aims: This study seeks at investigating the cause of hydrocephalus, and at identifying therapeutic targets for the prevention of hydrocephalus. ***Results:*** In this study, we show that inactivation of the Foxo3a gene in two mouse models of Fanconi anemia (FA) leads to the development of hydrocephalus in late embryonic stage and after birth. More than 50% of Foxo3a$^{-/-}$ Fancc$^{-/-}$ or Foxo3a$^{-/-}$ Fancd2$^{-/-}$ mice die during embryonic development or within 6 months of life as a result of hydrocephalus characterized by cranial distortion, dilation of the ventricular system, reduced thickness of the cerebral cortex, and disorganization of the ependymal cilia and subcommissural organ. Combined deficiency of Foxo3a and Fancc or Fancd2 not only impairs the self-renewal capacity but also markedly increases the apoptosis of neural stem and progenitor cells (NSPCs), leading to defective neurogenesis. Increased accumulation of reactive oxygen species (ROS) and subsequently de-regulated mitosis and ultimately apoptosis in the neural stem or progenitor cells is identified as one of the potential mechanisms of congenital obstructive hydrocephalus. ***Innovation:*** The work unravels a two-tier protective mechanism for preventing oxidative stress-induced hydrocephalus. ***Conclusion:*** The deletion of *Foxo3a* in FA mice increased the accumulation of ROS and subsequently de-regulated mitosis and ultimately apoptosis in the NSPCs, leading to hydrocephalus development. *Antioxid. Redox Signal.* 21, 1675–1692.

Introduction

HYDROCEPHALUS, a common birth defect affecting 1–3 of every 1000 live births, is characterized by the increased cerebrospinal fluid (CSF) volume and dilation of cerebral ventricles (2). The development of hydrocephalus is a dynamic process that is not yet well understood. It is thought that hydrocephalus may develop at an important and specific embryonic time period of neural stem cell (NSC) and progenitor cell proliferation and differentiation in the brain. Indeed, recent reports indicate that survival and proliferation of the NSC and progenitor cells within the ventricular zone lining the lateral ventricle (LV) are deregulated during hydrocephalic development (19, 53). Multiple transcriptional regulators have been implicated in the altered homeostasis of

Innovation

Hydrocephalus is a common birth defect affecting 1–3 of every 1000 live births. The genetic and environmental factors are mostly unknown. Our work shows that, in mouse models of Fanconi anemia, a childhood disease with high hydrocephalus penetration, inactivation of a major cellular antioxidant defense pathway leads to the development of hydrocephalus. Our findings reveal a novel interaction between the cellular antioxidant defense and DNA repair pathways. New insights into the potential integration of DNA repair proteins in oxidative-stress signaling pathways can suggest new targets for therapeutic prevention and treatment of developmental diseases, such as hydrocephalus.

[1]Division of Experimental Hematology and Cancer Biology, Cincinnati Children's Hospital Medical Center, Cincinnati, Ohio.
[2]Department of Neurosurgery, University of California, San Diego, La Jolla, California.
[3]Division of Bone Marrow Transplant and Immune Deficiency, Cincinnati Children's Hospital Medical Center, Cincinnati, Ohio.
[4]Department of Pediatrics, University of Cincinnati College of Medicine, Cincinnati, Ohio.

Table 1. Survival of *Foxo3a*$^{-/-}$ *Fancd2*$^{-/-}$ Embryos and Pups

Foxo3a$^{+/-}$ Fancd2$^{+/-}$ × Foxo3a$^{+/-}$ Fancd2$^{+/-}$ *intercross*				
	Foxo3a$^{-/-}$ Fancd2$^{+/+}$ *or* Foxo3a$^{-/-}$ Fancd2$^{+/-}$	Foxo3a$^{+/+}$ Fancd2$^{-/-}$ *or* Foxo3a$^{+/-}$ Fancd2$^{-/-}$	Foxo3a$^{-/-}$ Fancd2$^{-/-}$	*Other genotypes*
E13.5 embryos (98 screened)				
Expected	18	18	6	56
Observed	20	16	5 ($p = 0.834$)	57
Live pups (482 screened)				
Expected	90	90	30	272
Observed	95	86	17 ($p = 0.011$)[a]	284

[a]Significant at $p < 0.05$.

NSC and progenitor cells that are associated with hydrocephalus. These factors include Engrailed 1, Msx1, E2F5, RFX4, Foxj1/Hfh-4, polymerase λ, and, more recently, KLF4 (25, 44).

Mammalian forkhead members of the class O (FOXO) transcription factors, including FOXO1, FOXO3, FOXO4, and FOXO6, are implicated in the regulation of cell-cycle arrest, apoptosis, DNA repair, stress resistance, and metabolism (4). Mouse knockout studies have shown that Foxo factors, particularly Foxo3a, function to regulate the self-renewal of hematopoietic stem cells, primarily by providing resistance to oxidative stress (24, 54). In the context of mammalian brain physiology, combined Foxo1, 3, and 4 deficiencies severely impair NSC proliferation and renewal, leading to a significant decline in the NSC pool and accompanying defective neurogenesis in adult brains (41). Among these FOXO proteins, FOXO3 functions as a major regulator of oxidative stress by activating genes involved in the free radical scavenging and apoptosis (55). A recent study by Renault *et al.* (45) demonstrates that deletion of *Foxo3a* alone in the brain is sufficient to cause a significant decline in NSC pool and that NSCs isolated from adult Foxo3$^{-/-}$ mice have decreased self-renewal and an impaired ability to generate different neural lineages. We recently reported a functional interaction between FOXO3 and the Fanconi anemia (FA) protein FANCD2 in response to oxidative stress (34). The role of the FA DNA repair pathway in mammalian brain physiology is less understood. One study reported that adult mice deficient for *Fanca* or *fancg* exhibited reduced proliferation of neural progenitor cells, and both embryonic and adult FA NSCs showed impaired self-renewal *in vitro* (49). In this study, we present evidence that concomitant inactivation of Foxo3a and Fancc or Fancd2 synergizes and induces hydrocephalus in mice.

FA is a genetic disease that is characterized by genomic instability and cancer predisposition (29). FA is caused by a deficiency in any of the 15 *FANC* genes that designate complementation group *A* to *P* (30). At least 90% of affected FA patients show one or more malformations, including radial ray defects; genital, renal, and urinary tract abnormalities; and cardiac malformations (50). Cases of hydrocephalus in children with FA have been reported (21, 31, 35). FA patients suffer from a pro-oxidant state that is associated with overproduction or impaired detoxification of reactive oxygen species (ROS) (11, 13). As a consequence, cells from FA patients demonstrate hypersensitivity to ambient oxygen and increased chromosomal aberrations (8, 25). FA oxidant hypersensitivity has been documented in many studies using primary and immortalized cell cultures as well as *ex vivo* materials from patients (9, 11, 27). We hypothesized that oxidative stress might be a critical factor in the pathogenesis of FA hydrocephalus. To test this, we inactivated Foxo3a to induce physiological oxidative stress in two FA mouse models, and report here that the deletion of *Foxo3a* in FA mice increased accumulation of ROS and subsequently deregulated mitosis and ultimately apoptosis in the NSCs and progenitor cells in FA hydrocephalic mice.

Results

Deletion of Foxo3a *in FA mice leads to embryonic lethality and hydrocephalus*

To further elucidate the genetic relationships between the *Foxo3a* and FA pathways, we generated *Foxo3a*$^{-/-}$ *Fancd2*$^{-/-}$ and *Foxo3a*$^{-/-}$ *Fancc*$^{-/-}$ mice by crossing *Foxo3a*$^{+/-}$ with *Fancd2*$^{+/-}$ or *Fancc*$^{+/-}$ mice, respectively. Screening more than 200 E13.5 embryos indicated an expected Mendelian ratio for either single knockout (SKO) or

FIG. 1. Deletion of *Foxo3a* in FA mice leads to embryonic lethality and hydrocephalus. (A) A representative image of E13.5 littermates from a *Foxo3a*$^{+/-}$ *Fancd2*$^{+/-}$ breeder and genotyping of the embryos. **(B)** The body weight of 6-week-old WT, *Fancd2*$^{-/-}$ SKO, *Foxo3a*$^{-/-}$ SKO, and *Foxo3a*$^{-/-}$ *Fancd2*$^{-/-}$ DKO mice. **(C)** Nissl staining of serial rostral (r) to caudal (c) coronal sections of E18.5 brain with each pair of sections representing approximately the same coronal plane. **(D)** Dome-shaped head was shown in both *Foxo3a*$^{-/-}$ *Fancd2*$^{-/-}$ and *Foxo3a*$^{-/-}$ *Fancc*$^{-/-}$ DKO mice. **(E)** MRI and CT scanning of WT, *Fancd2*$^{-/-}$ SKO, *Foxo3a*$^{-/-}$ SKO, and *Foxo3a*$^{-/-}$ *Fancd2*$^{-/-}$ DKO mice. The DKO mouse showed increased CSF volume, enlarged LV, and increased diameter of brain skull. **(F)** Nissel staining of the coronal adult brain sections of the WT, *Fancd2*$^{-/-}$ SKO, *Foxo3a*$^{-/-}$ SKO, and *Foxo3a*$^{-/-}$ *Fancd2*$^{-/-}$ DKO mice. LV, lateral ventricle; 3V, third ventricle; Hi, hippocampus; Cx, cortex; CSF, cerebrospinal fluid; FA, Fanconi anemia; DKO, double knockout; SKO, single knockout; WT, wild type; MRI, magnetic resonance imaging; CT, computerized tomography. To see this illustration in color, the reader is referred to the web version of this article at www.liebertpub.com/ars

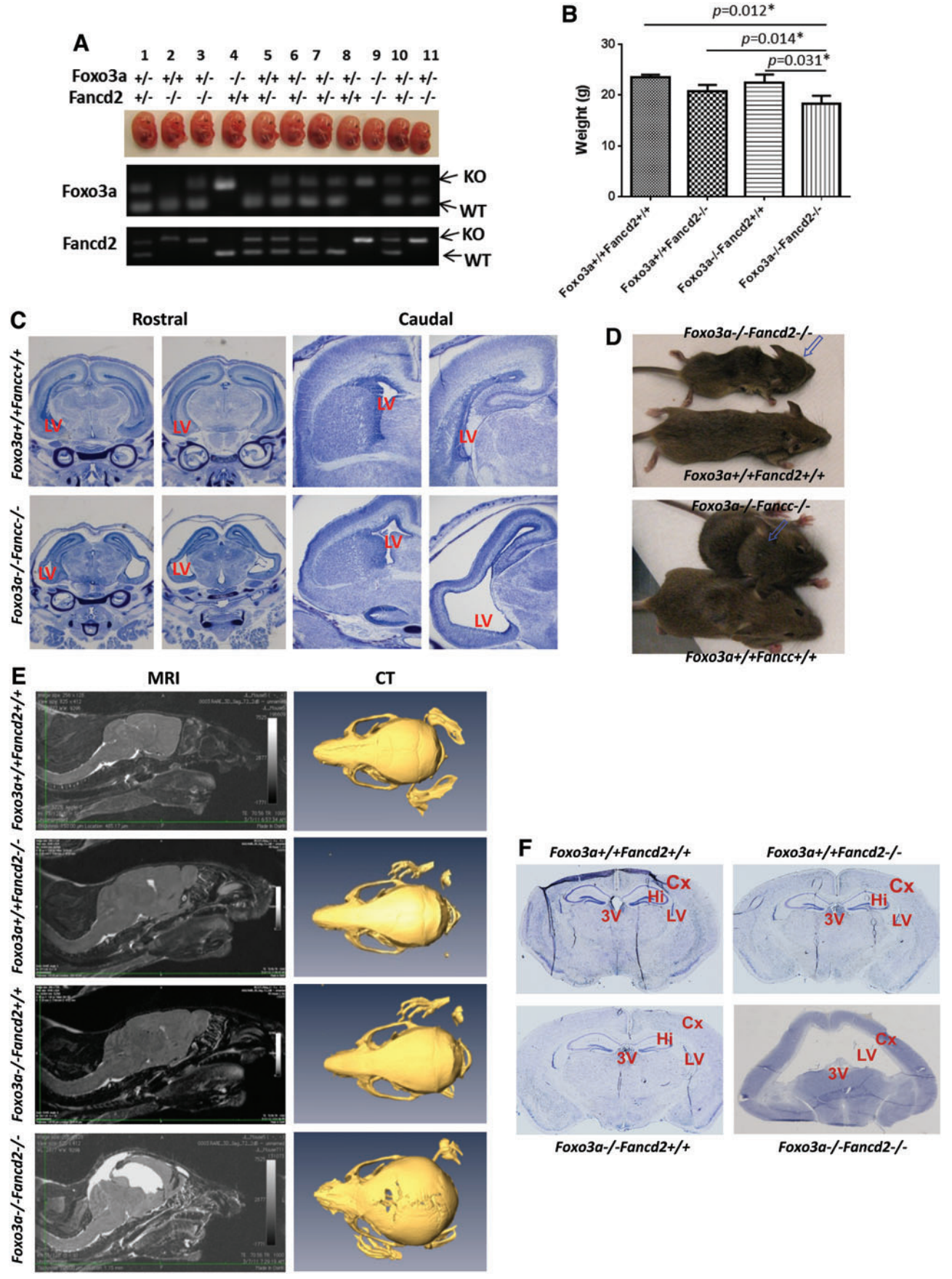
A
1 2 3 4 5 6 7 8 9 10 11
Foxo3a +/- +/+ +/- -/- +/+ +/- +/- +/- -/- +/- +/-
Fancd2 +/- -/- -/- +/+ +/- +/- +/- +/+ -/- +/- -/-
Foxo3a
KO
WT
Fancd2
KO
WT
B
p=0.012*
p=0.014*
p=0.031*
Weight (g)
30
20
10
0
Foxo3a+/+Fancd2+/+
Foxo3a+/+Fancd2-/-
Foxo3a-/-Fancd2+/+
Foxo3a-/-Fancd2-/-
C
Rostral
Caudal
Foxo3a+/+Fancc+/+
Foxo3a-/-Fancc-/-
LV
D
Foxo3a-/-Fancd2-/-
Foxo3a+/+Fancd2+/+
Foxo3a-/-Fancc-/-
Foxo3a+/+Fancc+/+
E
MRI
CT
Foxo3a+/+Fancd2+/+
Foxo3a+/+Fancd2-/-
Foxo3a-/-Fancd2+/+
Foxo3a-/-Fancd2-/-
F
Foxo3a+/+Fancd2+/+
Foxo3a+/+Fancd2-/-
Cx
Hi
3V
LV
Foxo3a-/-Fancd2+/+
Foxo3a-/-Fancd2-/-

double knockout (DKO) offspring (Table 1; $p=0.834$ and Supplementary Table S1; Supplementary Data are available online at www.liebertpub.com/ars; $p=0.846$). However, of the 804 live pups analyzed, 29 *Foxo3a*$^{-/-}$ *Fancd2*$^{-/-}$ or *Foxo3a*$^{-/-}$ *Fancc*$^{-/-}$ DKO mice were obtained, which was 58% of the expected live births (Table 1; $p=0.011$ and Supplementary Table S1; $p=0.035$). This suggests that about 40% of the DKO embryos died from embryonic day E13.5 to birth. DKO embryos were smaller relative to their wild-type (WT) or SKO littermates at E13.5 (Fig. 1A and Supplementary Fig. S1A). In addition, DKO pups were significantly smaller than control littermates (Fig. 1B and Supplementary Fig. S1B), while the SKO pups were similar to the WT pups (Supplementary Fig. S1C). These data indicate that although defects in *Foxo3a*, *Fancd2*, or *Fancc* individually are compatible with grossly normal development and organismal viability, simultaneous defects in *Foxo3a* and *Fancd2* or *Fancc* cause synthetic lethality.

Approximately 60% of DKO embryos had abnormal brain structure that was characteristic of hydrocephalus (Fig. 1C and Supplementary Fig. S1D). Coronal sections revealed dilated LVs with a disruption of the septum, which was evident in as early as E18.5 (Fig. 1C). About 30%–50% of the DKO mice exhibited hydrocephalus and died within 6 months of birth. The mice with hydrocephalus developed a dome-shaped head and behavioral changes that included weight loss, lethargy, and ruffled fur (Fig. 1D). Hydrocephalus was confirmed in these mice by magnetic resonance imaging (MRI) and computerized tomography (CT) scanning (Fig. 1E). MRI images showed that the CSF volume and the dilation of the cerebral ventricle in the dome-shaped head of DKO mice was obviously increased compared with that in WT or SKO mice (Fig. 1E, left). CT scanning revealed a significant increase in the diameters of the DKO mice brain skull (Fig. 1E, right). Nissel staining of the serial brain sections showed that DKO mice with hydrocephalus had enlarged LVs, agenesis of the hippocampus, and thinner cerebral cortex compared with WT or SKO mice (Fig. 1F).

Decreased neural stem and progenitor cells in DKO mice

Loss of neural stem and progenitor cells (NSPCs) has been shown to be associated with hydrocephalus (44, 53). We, thus, determined the number of NSPCs in the ventricle zone (VZ) and subventricular zone (SVZ) by staining the brain of E13.5 embryos with Sox2 (established NSPC marker), and Tbr2 (intermediate progenitor cell marker) (1, 48). We found that the number of NSPCs in the VZ and SVZ area of the DKO mice was significantly decreased compared with that of WT controls (Fig. 2A). To determine whether reduced NSPCs in DKO brains lead to impaired neurogenesis, we examined neuronal cell differentiation/migration in the cortex, as cortical neurons are generated within the VZ and migrate into the cortex (38). We stained the later born upper and the earlier born deep layers of the cortex with the layer-specific markers. Both the upper layer, identified by Cux1/2 staining (39), and the deep layer, stained with Foxp2 (15), were significantly reduced compared with the WT control brains (Fig. 2B). Thus, the thinning in the cortical layers of the DKO brains may result from the loss of NSPCs.

To further assess the consequence of NSPC loss in the context of hydrocephalus in DKO mice, we examined ependymal cells, which are derived from NSPCs during later embryogenesis and develop cilia in the first postnatal week (51). Defects in the structure and activity of ependymal cilia have been shown to associate with hydrocephalus in humans and mouse models (16). Staining for cilia in the VZ with acetylated α-tubulin showed that bundles of motile cilia protruded into the LV lumen in the WT brains. Although the acetylated α-tubulin in DKO mice could still be identified, there were a few cilia on ependymal cells lining the LV (Fig. 2C). In addition, the cilia in DKO mice were much shorter and disorganized than that in the WT littermates (Fig. 2C). We also examined the subcommissural organ (SCO), which is composed of ependymal cells and participates in the circulation and re-absorption of CSF. Destruction of the SCO leads to obstructive hydrocephalus (43). The size of SCO was significantly reduced in the DKO mice compared with that in the WT controls (Fig. 2D). These data suggest that defective SCO and ependymal cilia may be a direct cause of hydrocephalus in DKO mice.

DKO NSCs have increased ROS and decreased self-renewal potential

To gain insights into the mechanism behind the NSPC loss in hydrophilic DKO mice, we performed gene expression profiling using an Affymetrix gene array platform on RNA isolated from WT, SKO, and DKO mice brain tissues. A microarray analysis revealed 366 up-regulated genes and 360 down-regulated genes in DKO mice, 249 up-regulated and 439 down-regulated genes in *Fancd2* SKO mice, and 313 up-regulated and 409 down-regulated genes in *Foxo3a* SKO mice, with ≥1.3-fold increase or decrease. Analysis of the microarray data revealed that oxidative phosphorylation and mitochondrial dysfunction (such as Ndufa1, Ndufb8, Cox4i1, Cox5b, Cox7a2 Cox7a2l, Cyc1, Uqcrc1, Uqcrfs1, Atp5o, Sdhc, Bcs1l, Atp5e, and Atp5l) (36) were altered in the Foxo3 SKO and DKO mouse (Fig. 3A, B), which was consistent with the function of FOXO3 proteins in anti-oxidative defense (41). In addition, a specific subset of genes encoding

FIG. 2. Decreased NSPCs in *Foxo3a*$^{-/-}$ *Fancd2*$^{-/-}$ DKO mice. (A) Sox2 and Tbr2 staining of the coronal brain sections from WT, SKO, and DKO E13.5 embryos. Scale bar represents 50 μm. The bar graph (*right*) shows quantitation of SOX2-positive cells in the VZ area ($n=5$). **(B)** The thickness of upper layer cortex (stained by Cux1/2) and deeper layer cortex (stained by Foxp2) in the WT, SKO, and DKO E18.5 embryos was measured ($n=5$). Scale bar represents 25 μm. **(C)** Ependymal cilia were examined at P5 by staining for Ac-tubulin. Scale bar represents 20 μm. **(D)** Representative DAPI staining of the SCO of WT, SKO, and DKO E18.5 embryos, and quantitation showing a greatly reduced size of the SCO of DKO brain ($n=5$). Scale bar represents 100 μm. Quantitation is compared between WT, SKO, and DKO embryos ($n=5$). *$p<0.05$; **$p<0.01$. NSPC, neural stem and progenitor cell; Ac-tubulin, acetylated α-tubulin; SCO, subcommissural organ; VZ, ventricle zone. To see this illustration in color, the reader is referred to the web version of this article at www.liebertpub.com/ars

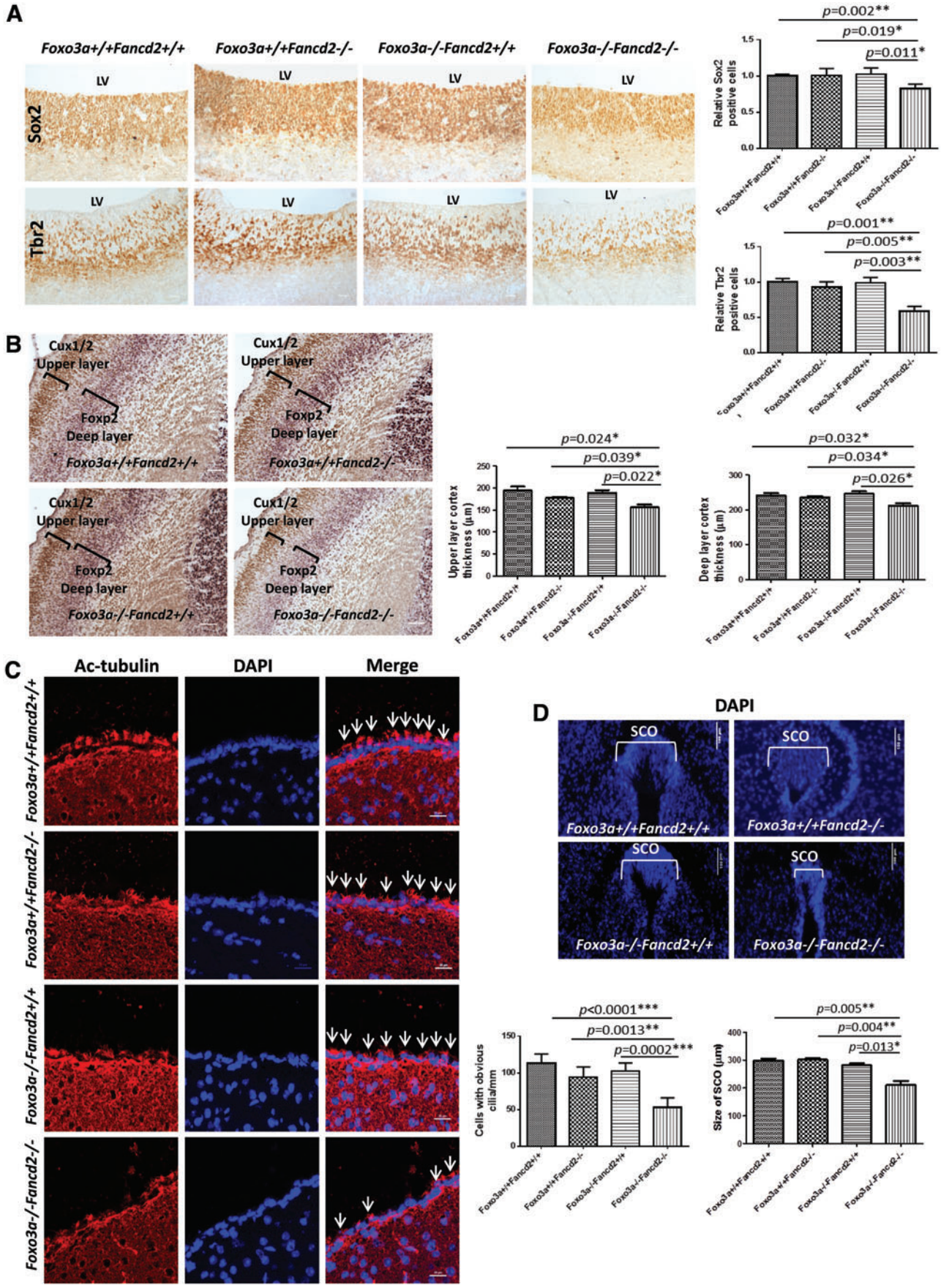
A
Foxo3a+/+Fancd2+/+
Foxo3a+/+Fancd2-/-
Foxo3a-/-Fancd2+/+
Foxo3a-/-Fancd2-/-
LV
Sox2
Tbr2
p=0.002**
p=0.019*
p=0.011*
Relative Sox2 positive cells
p=0.001**
p=0.005**
p=0.003**
Relative Tbr2 positive cells
B
Cux1/2
Upper layer
Foxp2
Deep layer
p=0.024*
p=0.039*
p=0.022*
Upper layer cortex thickness (μm)
p=0.032*
p=0.034*
p=0.026*
Deep layer cortex thickness (μm)
C
Ac-tubulin
DAPI
Merge
D
DAPI
SCO
p<0.0001***
p=0.0013**
p=0.0002***
Cells with obvious cilia/mm
p=0.005**
p=0.004**
p=0.013*
Size of SCO (μm)

molecules known to regulate NSPC proliferation and neurogenesis (such as Ntf3, Mll1, bglap, Bmpr1b, Lbx1, and Hdac1) (42, 59) was substantially down-regulated in the DKO mouse. Moreover, the brain of DKO mice showed dysregulated transcription of genes involved in aging and neurological disorders (such as S100b, Serpina3, Mog, and Uchl1) (3, 10, 12, 17, 28, 32) (Fig. 3A, B and Supplementary Fig. S2).

To determine whether DKO mice suffer oxidative stress, we measured the levels of ROS in the NSPCs and 6-week-old brains. The results showed that ROS production in the NSPCs of DKO embryos was significantly increased compared with that of WT mice (Fig. 4A; $p<0.01$). The level of ROS in Foxo3a$^{-/-}$ NSPCs was also significantly higher than that of WT mice ($p<0.05$), which was consistent with previous reports (41). Similar results were obtained in the 6-week-old mouse brain tissues (Supplementary Fig. S3A).

To assess the consequence of ROS over-production, we analyzed the proliferation and renewal of NSCs isolated from E12.5 embryos of WT, SKO, and DKO mice by using well-established cell culture-based approaches. NSCs from Foxo3a or Fancd2 SKO mice formed fewer (albeit not statically significant) multipotent neurospheres in culture than WT NSCs (Fig. 4B; Supplementary Fig. S3B). This phenotype was significantly enhanced in the NSCs from DKO mice, which on average formed 1.8-fold fewer neurospheres than WT NSCs (Fig. 4B; $p<0.01$). The neurospheres formed by the DKO NSCs were significantly smaller than the neurospheres of SKO and WT controls (Fig. 4C; $p<0.01$). Consistent with this, BrdU incorporation in these NSC cultures revealed that DKO NSCs had decreased proliferation when compared with WT and SKO NSCs (Fig. 4D; $p<0.05$ or $p<0.01$). The self-renewal potential of the DKO NSCs, as judged by the number of multipotent secondary neurospheres that arose per primary neurosphere, exhibited a dramatically reduced culture as compared with the NSCs of SKO or WT littermate controls (Fig. 4E). These data demonstrate that simultaneous defects in *Foxo3a* and *Fancd2* exacerbate the SKO deficiency in proliferation and self-renewal of NSCs in clonal culture.

To validate the effect of ROS on NSC homeostasis, we fed WT and *Foxo3a*$^{-/-}$ *Fancd2*$^{-/-}$ DKO mice with a specialized diet containing Quercetin (3,5,7,3′,4′-pentahydroxyflavone; Fig. 5A), a natural ROS scavenger. We observed that heterozygous *Foxo3a*$^{+/-}$ *Fancd2*$^{+/-}$ breeders on Quercetin diet gave birth to higher numbers of DKO offspring than the *Foxo3a*$^{+/-}$ *Fancd2*$^{+/-}$ breeders on normal diet (Table 2), indicating rescue of embryonic lethality by the antioxidant. Moreover, Quercetin significantly reduced hydrocephalus-related death of the DKO pups by more than twofold (Table 2). The nissel staining of brain sections of the Quercetin-fed mice showed that the size of LV of DKO mice was similar to that of WT mice (Supplementary Fig. S4A). SVZ tissues isolated from DKO offspring continued on Quercetin food for 8 weeks exhibited obviously decreased ROS levels (Fig. 5B). Staining brain sections with antibodies to NSPC marker Sox2 revealed that the 8-week-old DKO brain on Quercetin experienced a significant increase in Sox2-positive cells in the SVZ compared with DKO mice on a normal diet (Fig. 5C). Quercetin-fed DKO mice also showed a marked increase in proliferation of NSCs, as analyzed by staining the SVZ cells with antibodies for Ki67 (Fig. 5D). Consistent with this, neurospheres formed by SVZ cells from Quercetin-fed DKO mice exhibited a significant increase in average diameter compared with normal diet controls (Fig. 5E; 176.8 μm *vs.* 102.3 μm, $p=0.024$). Furthermore, the neurosphere number per SVZ area from Quercetin-fed DKO mice was nearly twofold more than that of normal-diet-fed mice (Fig. 5F). We observed a similar effect of another antioxidant, *N*-acetylcysteine (NAC), in *in vitro* NSC culture experiments (Supplementary Fig. S4B–E). Together, these results support the notion that increased ROS accumulation contributes to impaired proliferation and self-renewal potential of DKO NSCs. Thus, Foxo3a and the FA proteins may act cooperatively to support NSC homeostasis *in vivo*, probably by preventing cellular damage caused by high levels of ROS.

Increased DNA damage, apoptosis, and mitosis in DKO NSCs

To further investigate the cause of NSC depletion in DKO mice, we examined three cellular events that are most relevant to ROS in NSCs: DNA damage, apoptosis, and cell-cycle checkpoint. We performed γ-H2AX staining on neurospheres formed by WT, *Foxo3a*$^{-/-}$ SKO, *Fancd2*$^{-/-}$ SKO, and *Foxo3a*$^{-/-}$ *Fancd2*$^{-/-}$ DKO NSCs, and quantified the frequency of NSCs containing at least five γ-H2AX foci, an established marker of DNA damage. There was a significant increase in γ-H2AX foci, indicative of DNA damage in DKO NSCs when compared with either the WT or SKO group (Fig. 6A). Flow cytometric analysis of Annexin V-labeled cells revealed increased apoptosis in DKO NSCs (Fig. 6B). We reasoned that the apparent increase in DNA damage and apoptosis in DKO NSCs could be due to checkpoint activation and, therefore, examined the cell-cycle status by labeling the NSCs with BrdU in the S phase. DKO NSCs showed a reduction in the S phase but an increase in the G2/M phase when compared with the WT or SKO NSCs (Fig. 6C). Staining of E18.5 embryo brain sections with phospho-histone H3 (pHH3), which is present in late G2/M phase of the cell cycle, showed a marked increase in dividing (pHH3-positive) cells at the ventricular surface of cortices in DKO brains at E18.5; while in WT control brains, very few dividing cells could be seen along the ventricular surface (Fig. 6D). Together, these findings suggest that ROS-mediated proliferation and self-renewal defects of DKO NSCs are associated with the accumulation of DNA damage, de-regulated mitosis, and, ultimately, apoptosis.

DKO NSCs display mitotic catastrophe

To gain insights into the molecular mechanisms that are responsible for increased DNA damage, mitosis, and apoptosis in DKO NSCs, we revisited the genome-wide microarray data. We found that some mitotic catastrophe-related genes (57) were down-regulated in DKO NSCs when compared with the WT or SKO controls (Fig. 7A). For example, the depletion of HDACs can exacerbate DNA damage-induced mitotic catastrophe (18, 33). The down-regulation of spindle checkpoint proteins Bub1b or Aurkb has been shown to activate mitotic catastrophe *in vitro* (58). The changes in expression levels of these genes were validated by reverse transcription followed by quantitative polymerase chain reaction (PCR) (Supplementary Fig. S5A). We also performed two sets of experiments to validate the effect of these genes.

A

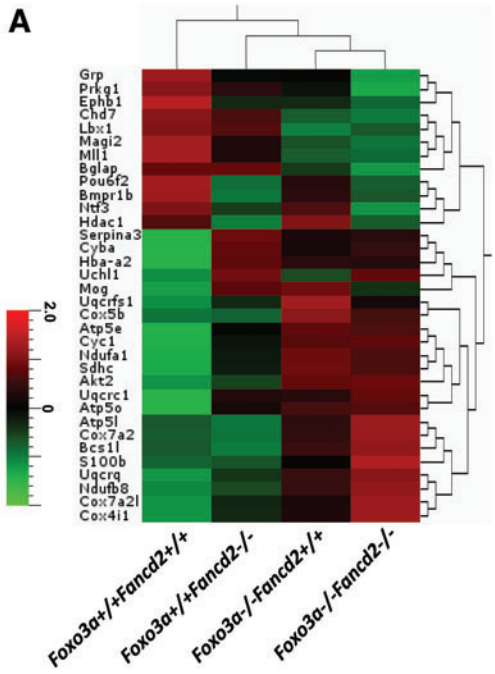

B

Molecular signature names	*Foxo3a-/-Fancd2-/-* VS *Foxo3a+/+Fancd2+/+*			*Foxo3a-/-Fancd2+/+* VS *Foxo3a+/+Fancd2+/+*			*Foxo3a+/+Fancd2-/-* VS *Foxo3a+/+Fancd2+/+*		
Neurological disorder	**No.**	**P-Value**	**Q-Value**	**No.**	**P-Value**	**Q-Value**	**No.**	**P-Value**	**Q-Value**
PARKINSONS_DISEASE	15	1.48E-13	1.28E-10	11	7.55E-09	9.63E-07	N/A	N/A	N/A
HUNTINGTONS_DISEASE	14	2.19E-10	7.60E-08	N/A	N/A	N/A	N/A	N/A	N/A
ALZHEIMERS_DISEASE_UP (REF 35)	34	3.90E-07	2.96E-05	39	1.27E-09	2.53E-07	66	0.00E+00	0.00E+00
Aging									
AGING_UP (REF 39)	7	2.17E-07	1.79E-05	N/A	N/A	N/A	8	6.25E-08	3.57E-06
AGING_NEOCORTEX_UP (REF 40)	8	4.53E-07	3.33E-05	N/A	N/A	N/A	N/A	N/A	N/A
Mitochondrial function									
RESPIRATORY_ELECTRON_TRANSPORT_ATP_SYNTHESIS	10	4.76E-09	9.61E-07	8	4.53E-07	2.42E-05	N/A	N/A	N/A
MITOCHONDRIA (REF 32)	18	1.56E-08	2.16E-06	N/A	N/A	N/A	N/A	N/A	N/A
TCA_CYCLE_AND_RESPIRATORY_ELECTRON_TRANSPORT	10	1.57E-07	1.38E-05	N/A	N/A	N/A	N/A	N/A	N/A
RESPIRATORY_ELECTRON_TRANSPORT	8	1.79E-07	1.55E-05	N/A	N/A	N/A	N/A	N/A	N/A
Oxidative phosphorylation									
VOXPHOS (REF 32)	11	7.66E-11	3.10E-08	8	3.80E-07	2.12E-05	N/A	N/A	N/A
OXIDATIVE_PHOSPHORYLATION	11	8.83E-09	1.34E-06	N/A	N/A	N/A	N/A	N/A	N/A
Stem cell									
ADULT_TISSUE_STEM_MODULE (REF 33)	24	2.66E-09	5.61E-07	N/A	N/A	N/A	28	8.95E-10	8.35E-08
EMBRYONIC_STEM_CELL_CORE (REF 33)	13	2.36E-06	1.26E-04	N/A	N/A	N/A	N/A	N/A	N/A
MAMMARY_STEM_CELL_DN (REF 34)	10	2.17E-07	1.79E-05	N/A	N/A	N/A	N/A	N/A	N/A

FIG. 3. Deregulated expression of genes in ROS metabolism, mitochondrial function, stem cell proliferation, and neurogenesis in DKO brains. Whole-genome microarray data were obtained from 2-month-old WT, SKO, and DKO brain tissues. **(A)** Heat-map presentation of differentially expressed genes in altered pathway of neurogenesis, NSCs, neurological disorder, oxidative phosphorylation, and mitochondrial dysfunction in the DKO mouse brain. **(B)** Selected publicly available molecular signature highly enriched for genes up-regulated or down-regulated in DKO brain tissue as provided by GSEA (gene set enrichment analysis). ROS, reactive oxygen species; NSC, neural stem cell. To see this illustration in color, the reader is referred to the web version of this article at www.liebertpub.com/ars

First, we treated the NSCs isolated from WT and *Foxo3a*$^{-/-}$ *Fancd2*$^{-/-}$ DKO mice, with the Aurora B inhibitor, Reversine (5 μM) for 48 h, and determined the size and number of the neurospheres. The results show that Reversine further inhibited neurosphere formation of DKO NSCs (Supplementary Fig. S5B). Second, we overexpressed BubR1 in WT and DKO NSCs and determined whether BubR1 overexpression could rescue the defect of neurosphere formation of DKO NSCs. We observed a significant increase, albeit not complete rescue, in the proliferation of DKO NSCs (Supplementary Fig. S5C).

To determine whether DKO NSCs underwent mitotic catastrophe, we analyzed the neurospheres and NSC-containing VZ area of the brains of WT, *Foxo3a*$^{-/-}$ SKO, *Fancd2*$^{-/-}$ SKO, and *Foxo3a*$^{-/-}$ *Fancd2*$^{-/-}$ DKO NSCs for γ-H2AX, pHH3, and active caspase-3. The activation of mitotic catastrophe can be identified by the simultaneous appearance of DNA damage (monitored by γ-H2AX), mitotic markers (monitored by pHH3), and activation of caspase-3 (26). *Fancd2* SKO cells and brain showed an increase in γ-H2AX and cleaved caspase-3 staining compared with WT controls; however, no evidence of mitotic catastrophe was observed as indicated by the lack of positive triple staining cells (Fig. 7B–E and Supplementary Fig. S6A–C). Although *Foxo3a*$^{-/-}$ SKO cells accumulated high levels of ROS, these cells did not display increased staining for γ-H2AX foci or pHH3 or cleaved caspase-3, suggesting that the DNA damage and cell-cycle checkpoints remained largely intact in *Foxo3a*-deficient cells. In marked contrast, a large fraction of DKO NSCs and brains simultaneously exhibited positive staining for γ-H2AX, pHH3, and cleaved caspase-3 (Fig. 7E), consistent with the activation of mitotic catastrophe. Moreover, DKO cells showed increased micronuclei (Supplementary Fig. S6D), a product of chromosome mis-segregation often associated with mitotic catastrophe (46). Together, these data suggest a potential link between NSC loss and mitotic catastrophe in DKO mice.

Discussion

We have shown that, in mice deficient for the FA DNA repair pathway, inactivation of the *Foxo3a* gene caused hydrocephalus, a common birth defect clinically associated with the FA disease. The underlying mechanism likely involves ROS-induced DNA damage, leading to de-regulated mitosis and, ultimately, apoptosis of NSPCs in the VZ of DKO mice. Based on these findings, we propose a two-tier protective mechanism for preventing hydrocephalus (Fig. 7F): In the first line of defense, FOXO3 and other cellular antioxidant machinery prevent the accumulation of ROS generated by internal metabolism or external toxins. The second line of defense relies on the repair mechanisms that prevent cellular constituents, including DNA, proteins, and lipids from damage by ROS. In this context, FOXO3 and the FA pathway play critical roles at different levels of the defense. FOXO3 is a master ROS-responsive transcription factor that regulates the expression of several important antioxidant genes such as peroxiredoxins, glutathione peroxidases, and superoxide dismutases (SODs) (54). ROS can induce oxidative DNA damage, which is a major source of genomic instability. Several repair pathways, including the FA DNA repair pathway, are known to be involved in oxidative DNA repair (52). While the specificity and efficiency of each single pathway are critical to ensure genome stability, the complexity of ROS-induced oxidative DNA damage may require the coordination between different DNA repair pathways. We recently reported an oxidative DNA damage-specific association of FOXO3 and the FA protein FANCD2 (34), suggesting a functional cross-talk between the two pathways in this two-tier defense mechanism.

Hydrocephalus is caused by an abnormal accumulation of CSF within or around the brain, due to the obstruction of CSF flow, inadequate CSF absorption, and/or excessive CSF production. Little is known about the molecular mechanisms that are responsible for the pathophysiology of hydrocephalus. Several studies suggest a connection between hydrocephalus and oxidative stress. An analysis of congenitally hydrocephalic WIC-Hyd adult rat brains showed reduced levels of the anti-oxidative defense enzyme SOD in the ependyma, choroid plexus, and hippocampus (37). Two studies with the kaolin-induced hydrocephalic rat model showed increased brain lipid peroxide levels and reduced GSH levels after the induction of hydrocephalus (5, 56). Transgenic mice carrying mutations in the antioxidant vitamin E often succumb to hydrocephalus (22). Abnormal metabolism of metals, known to participate in oxidative cascades, is associated with hydrocephalus in farm animals (40). In humans, CSF from hydrocephalic children contains high levels of metabolites that are indicative of oxidative stress (47). In our DKO mice, the hydrocephalus phenotype caused by the defect in NSCs appeared around 1 month of age. We also found some defects in the bone marrow and testis (data not shown). However, the defect in NSCs is much more severe. Consequently, the phenotype of hydrocephalus shows up as early as E18.5 during development, indicating that the brain was most influenced by DKO. We found that ROS levels were significantly higher in the NSCs isolated from E12.5 DKO embryo and in the brains of E18.5 and

FIG. 4. *Foxo3a*$^{-/-}$ *Fancd2*$^{-/-}$ DKO NSCs show increased ROS and decreased self-renewal potential. **(A)** ROS production in WT, SKO, and DKO neurospheres isolated from E12.5 embryos. Cells were treated with DCF-DA, and ROS production was examined by flow cytometry. **(B)** Primary neurospheres formed by NSCs from E12.5 embryos of the indicated genotypes. The number of neurospheres formed 1 week after seeding was counted. Values represent mean ± SD from three independent experiments with $n = 5$ for each genotype. **(C)** Size of primary neurospheres described in **(B)**. Values represent mean ± SD from three independent experiments with $n = 5$ for each genotype. **(D)** Primary neurospheres were dissociated, single-cell suspensions were cultured for 24 h in medium that was supplemented with 10 μM BrdU, and level of BrdU incorporation was determined by BrdU immunostaining. Scale bar represents 100 μm. **(E)** Defective secondary neurosphere formation of DKO NSCs. Dissociated cells from the primary neurospheres described in **(B)** were cultured for 1 week, and the number of secondary neurospheres was counted. Values represent mean ± SD from three independent experiments with $n = 5$ for each genotype. *$p < 0.05$; **$p < 0.01$; and ***$p < 0.001$. DCF-DA, 2′-7′-dichlorofluorescein diacetate. To see this illustration in color, the reader is referred to the web version of this article at www.liebertpub.com/ars

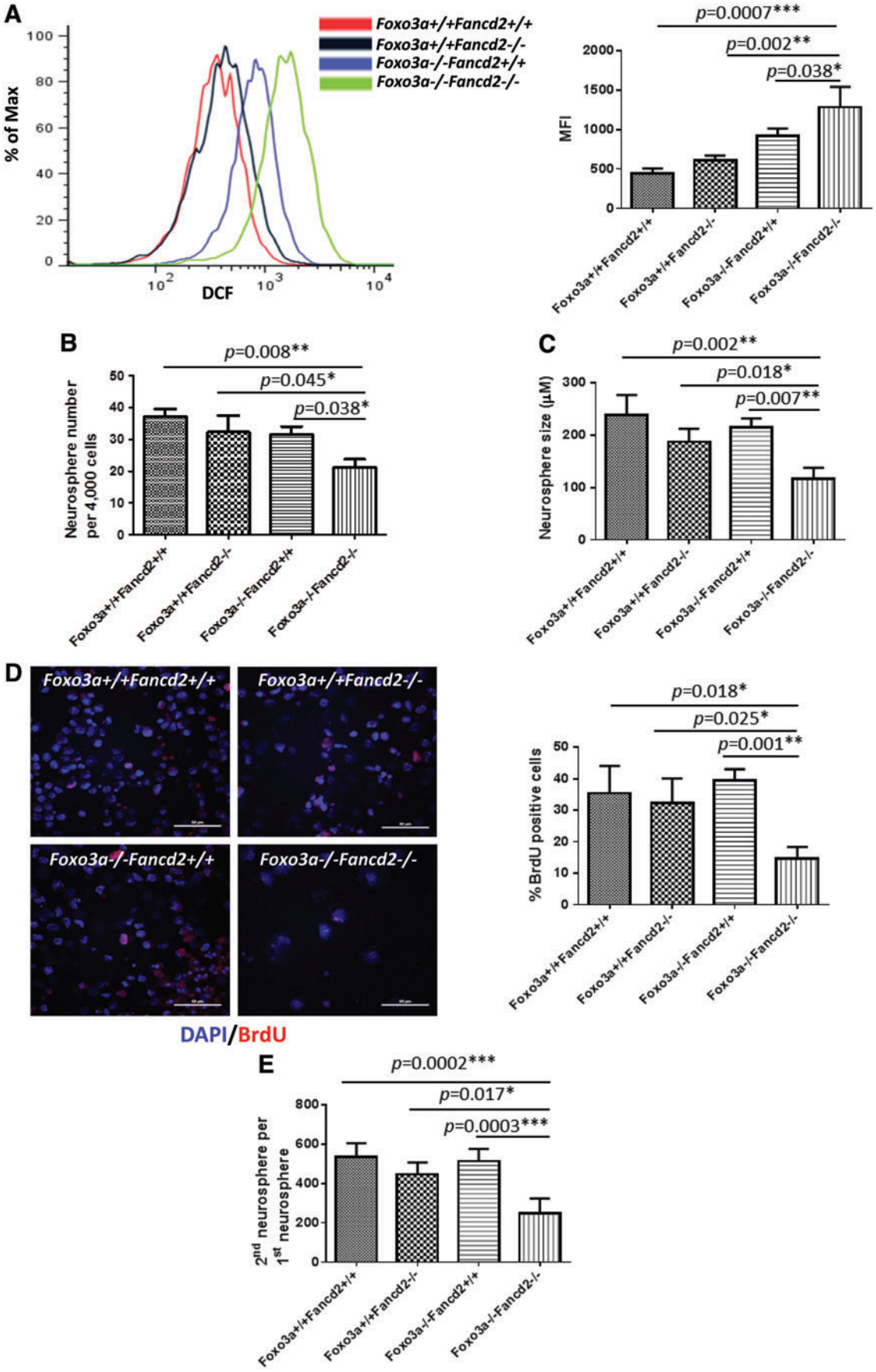
A
Foxo3a+/+Fancd2+/+
Foxo3a+/+Fancd2-/-
Foxo3a-/-Fancd2+/+
Foxo3a-/-Fancd2-/-
% of Max
DCF
p=0.0007***
p=0.002**
p=0.038*
MFI
B
p=0.008**
p=0.045*
p=0.038*
Neurosphere number per 4,000 cells
C
p=0.002**
p=0.018*
p=0.007**
Neurosphere size (µM)
D
DAPI/BrdU
p=0.018*
p=0.025*
p=0.001**
% BrdU positive cells
E
p=0.0002***
p=0.017*
p=0.0003***
2nd neurosphere per 1st neurosphere

6-week-old DKO mice. The antioxidants NAC and Quercetin reduced ROS accumulation in both NSCs and the brain of DKO mice. Importantly, Quercetin greatly ameliorated the synthetic lethality imposed by DKO *in utero* and completely eliminated hydrocephalus in DKO mice. These results indicate that, in DKO mice, oxidative stress is associated with the progression and molecular pathophysiology of hydrocephalus. This association suggests that oxidative brain damage may represent an important factor contributing to the pathogenesis of hydrocephalus. Excessive oxidative stress has been implicated in a number of adverse neurological conditions, including stroke, brain trauma, and neurodegenerative disease (14). Patients with FA may be particularly sensitive to oxidative stress because of an inherent defect in oxidative DNA damage repair and antioxidant defenses (13).

CSF is produced by the choroid plexus, a structure aligning the brain ventricles. We did not find abnormalities in this structure in the DKO mice. However, we observed a significant reduction in the size of SCO in the brain of DKO mice. Malformation of the SCO is considered the most common structural cause of hydrocephalus and has been implicated in the etiology of hydrocephalus in multiple transgenic mouse models (43). In addition to the SCO structure, the ependymal cilia in the ventricular zone play a critical role in maintaining the flow of CSF. Malformed cilia are associated with hydrocephalus in human patients (16). Several mouse models expressing mutations in genes encoding transcriptional regulators (Foxj1/Hfh-4, polymerase λ, and KLF4) or G-protein-coupled receptors (PAC1 and Ro1) show hydrocephalic phenotype as a consequence of defects in the ependymal cilia (25, 44). In the present study, we found that the cilia on the ventricular ependymal in DKO mice were either absent or much shorter and disorganized compared with those in the WT littermates. Since SCO and cilia originate from NSPCs in the VZ area and NSPC-derived ependymal cells, respectively, we speculate that abnormalities in both SCO and ependymal cilia in DKO mice may be a direct result of the defects of NSPCs. Indeed, we found that the number of SOX2-positive NSPCs in the VZ of E18.5 DKO embryos was significantly lower than that of WT controls. In addition, the reduction in NSPCs in the DKO brains led to impaired neurogenesis, as demonstrated by a significant reduction in the later born upper and the earlier born deep layers of the cortex compared with the WT control cortex. These results suggest that the abnormalities in the SCO and ependymal cilia observed in the DKO brains may be a result of the loss of NSPCs.

The fact that the occurrence of hydrocephalus in our model requires simultaneous inactivation of *Foxo3a* and *Fancd2* or *Fancc* genes indicates that the phenotype is a result of a synergistic effect similar to that of synthetic lethality imposed on DKO embryos. Since our comparative results from neurogenic studies in SKO and DKO mice point to a potential connection between hydrocephalus and NSC defects, we speculate a coordinate regulation of NSCs by the FOXO3 and FA pathways in two critical events in neurogenesis: self-renewal and apoptosis. Indeed, while *Foxo3a* or *Fancd2* SKO mice experienced a subtle decline in NSC number and self-renewal, NSCs isolated from E12.5 DKO embryos exhibited severe NSC deficiency. An analysis of the alteration in NSPC number in the embryonic brains and self-renewal in clonal culture revealed that the defect in DKO mice was not simply additive but synergistic, suggesting a collaborative action of these two pathways in NSC maintenance. FANCD2 protein can interact with several proteins, such as ataxia telangiectasia-mutated (ATM) protein (20) and FOXO3 (34). The handling of DNA damage caused by oxidative stress requires the coordinated action of FANCD2 and ATM (6). Moreover, FOXO3 can also interact with ATM (55) and is essential for normal ATM expression (61). FOXO3 represses ROS, in part, *via* regulation of ATM. Lacking FOXO3 did not trigger the DNA-repair mechanism after DNA damage (55). Overexpression of FOXO3 reduced abnormal accumulation of ROS, enhanced cellular resistance to oxidative stress, and increased antioxidant gene expression only in cells expressing a functional FANCD2 protein. This is in agreement with our observation that ROS-induced DNA damage and apoptosis was only slightly increased in the *Fancd2* or *Foxo3a* SKO NSCs but significantly increased in the DKO NSCs. This result suggests that Foxo3a and Fancd2 cooperate to affect the oxidative stress response. In support of this notion, gene array analysis revealed that the expression of genes involved in two major ROS signaling pathways, namely mitochondrial dysfunction and oxidative phosphorylation, was significantly altered in DKO mice compared with WT, Fancd2, or Foxo3a SKO mice.

An examination of brain sections and cultured NSPCs indicated that deficiencies in both *Foxo3a* and *Fancd2* genes

FIG. 5. Quercetin rescues embryonic lethality and NSC defects of DKO mice. (A) Chemical structure of Quercetin (3,5,7,3′,4′-pentahydroxy-flavone). **(B)** ROS production in the SVZ area of 2-month-old normal diet-feeding or Quercetin diet-feeding WT and *Foxo3a*$^{-/-}$ *Fancd2*$^{-/-}$ DKO mice. Cells were labeled with DCF-DA, and ROS production was examined by flow cytometry. *Right panel*, quantification of ROS levels in mice described in the *left panel* ($n=5$). **(C)** Sox2 staining of LV area of the 2-month-old normal diet-feeding or Quercetin diet-feeding WT and *Foxo3a*$^{-/-}$ *Fancd2*$^{-/-}$ DKO mice. Original magnification, $\times 20$; insert, $\times 40$. $\times 20$ scale bar: 100 μm; $\times 40$ scale bar: 50 μm. The bar graph (*right*) shows quantitation ($n=5$). Quercetin diet-feeding DKO mice demonstrated more SOX2-positive cells when compared with normal diet-feeding DKO mice. **(D)** Ki67-positive cells in the LV area of 2-month-old normal diet-feeding or Quercetin diet-feeding WT and *Foxo3a*$^{-/-}$ *Fancd2*$^{-/-}$ DKO mice. Scale bar represents 100 μm. *Bottom panel*, quantification of Ki67-positive cells in mice described in the *left panel* ($n=5$). Quercetin diet-feeding DKO mice demonstrated more Ki67-positive NSCs when compared with normal diet-feeding DKO mice. **(E, F)** Size and self-renewal ability of neurosphere from the SVZ area of 2-month-old normal diet-feeding or Quercetin diet-feeding WT and *Foxo3a*$^{-/-}$ *Fancd2*$^{-/-}$ DKO mice. Neurospheres formed by SVZ cells from Quercetin-fed DKO mice exhibited a significant increase in average diameter compared with normal diet-fed controls **(E; $n=5$)**. Scale bar represents 100 μm. The number of neurospheres formed by SVZ NSCs of Quercetin-fed DKO mice was twofold higher than the neurospheres derived from normal-diet-fed mice **(F; $n=5$)**. P2: S phase; P3: G1 phase; P4: G2/M phase. *$p<0.05$; **$p<0.01$; and ***$p<0.001$. SVZ, subventricular zone. To see this illustration in color, the reader is referred to the web version of this article at www.liebertpub.com/ars

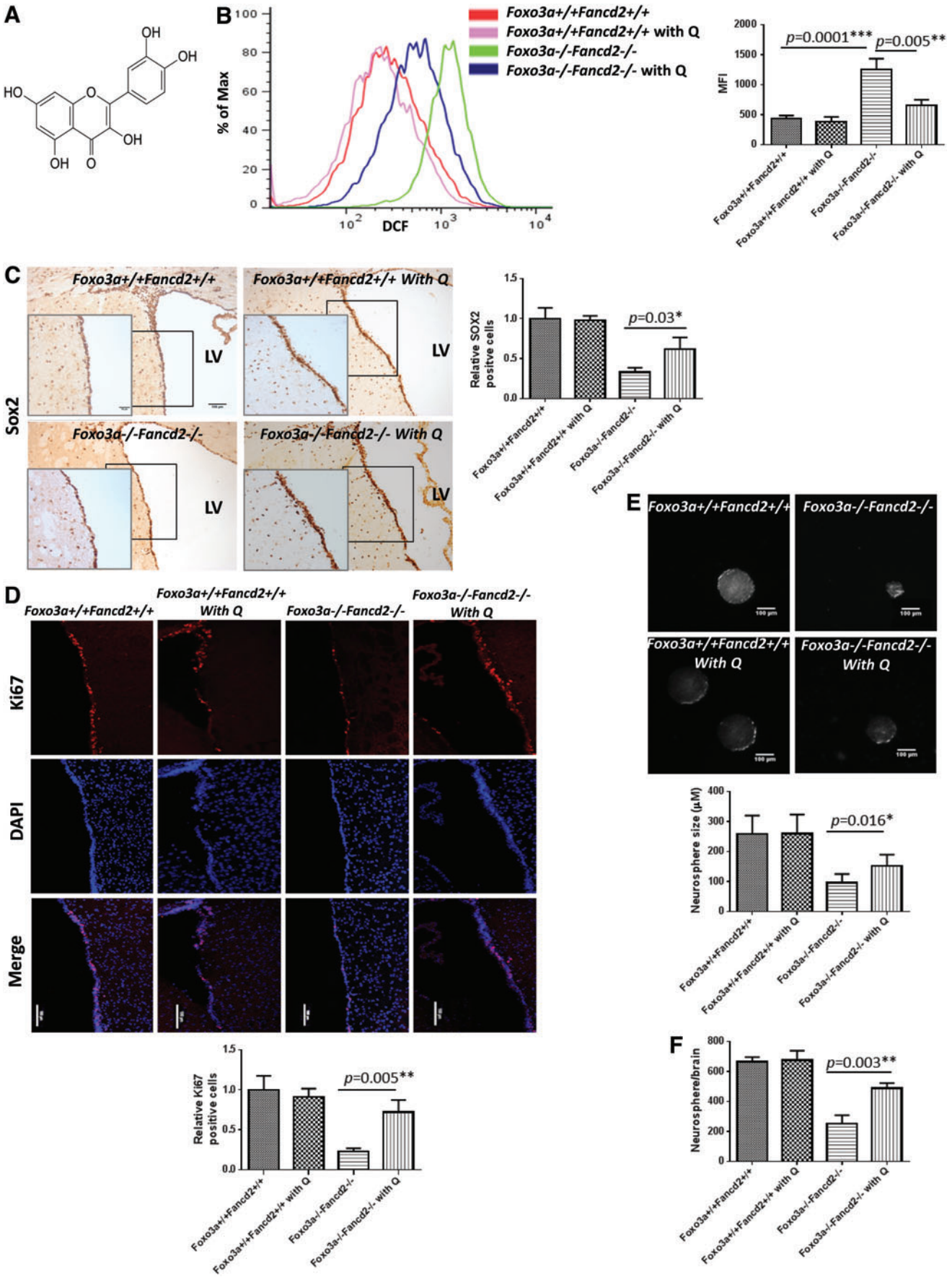
A
OH
OH
HO
O
OH
OH
O
B
Foxo3a+/+Fancd2+/+
Foxo3a+/+Fancd2+/+ with Q
Foxo3a-/-Fancd2-/-
Foxo3a-/-Fancd2-/- with Q
% of Max
DCF
p=0.0001***
p=0.005**
MFI
C
Foxo3a+/+Fancd2+/+
Foxo3a+/+Fancd2+/+ With Q
Foxo3a-/-Fancd2-/-
Foxo3a-/-Fancd2-/- With Q
LV
Sox2
p=0.03*
Relative SOX2 positve cells
D
Foxo3a+/+Fancd2+/+
Foxo3a+/+Fancd2+/+ With Q
Foxo3a-/-Fancd2-/-
Foxo3a-/-Fancd2-/- With Q
Ki67
DAPI
Merge
p=0.005**
Relative Ki67 positive cells
E
Foxo3a+/+Fancd2+/+
Foxo3a-/-Fancd2-/-
Foxo3a+/+Fancd2+/+ With Q
Foxo3a-/-Fancd2-/- With Q
p=0.016*
Neurosphere size (μM)
F
p=0.003**
Neurosphere/brain

Table 2. Quercetin Increases Birth and Survival of *Foxo3a*$^{-/-}$ *Fancd2*$^{-/-}$ Mice

Foxo3a$^{+/-}$ Fancd2$^{+/-}$ × Foxo3a$^{+/-}$ Fancd2$^{+/-}$ *intercross*		
	Normal diet Foxo3a$^{-/-}$ Fancd2$^{-/-}$	*Quercetin diet* Foxo3a$^{-/-}$ Fancd2$^{-/-}$
Birth (203 screened)		
Expected	12	12
Observed	7	10
p-Value	0.177	0.656
Survive (6 months) (203 screened)		
Expected	12	12
Observed	4	9
p-Value	0.010[a]	0.457

[a]Significant at $p < 0.05$.

are essential for the de-regulated mitosis and, ultimately, apoptosis. Mitotic catastrophe indicates cell death resulting from aberrant mitosis due to de-regulated cell-cycle checkpoint (26). ROS-induced DNA damage can be responsible for mitotically arrested cells that succumbed to mitotic catastrophe, which can be identified by simultaneous appearance of γ-H2AX, pHH3, and cleaved caspase-3 (26). Foxo3a SKO NSPCs accumulated ROS and exhibited positive staining for pHH3 but none of these cells showed γ-H2AX staining, indicating the preservation of functional DNA repair. Fancd2 SKO NSPCs generated low levels of ROS that correlated with sporadic γ-H2AX, pHH3, and caspase-3 staining, but no triple staining positive cells. ROS accumulation in these Fancd2 SKO NSPCs could be due to a requirement for the FA pathway to enable proper function of Foxo3a, or to facilitate access of Foxo3a to the promoters of anti-oxidative defense genes. Alternatively, a parallel anti-oxidative defense pathway that becomes less efficient in the absence of the FA pathway might be responsible for the ROS accumulation. We observed simultaneous expression of γ-H2AX, pHH3, and cleaved caspase-3, in cultured DKO neurospheres and NSPCs in the VZ area of DKO brains. Thus, loss of the FA DNA repair pathway in Foxo3a-deficient cells results in fatal DNA damage checkpoint abrogation, which enables the DKO cells to progress through the cell cycle despite the presence of unrepaired DNA damage. Taken together, these findings corroborate the notion that both anti-oxidative defense activity of Foxo3a and DNA repair function of the FA pathway are required for the prevention of de-regulated mitosis and, ultimately, apoptosis. DNA damage-induced de-regulated mitosis and apoptosis appears to be exacerbated by the inhibition of factors functioning in cytokinesis such as histone deacetylases, BubR1, and Aurora B (57). Intriguingly, our gene array data show that the expression of these cytokinesis genes was markedly reduced in the DKO mice. In addition, our data (Supplementary Fig. S6D) show that DKO cells exhibit increased micronuclei, a product of chromosome mis-segregation, consistent with de-regulated mitosis and failed cytokinesis.

Materials and Methods

Animals

The protocols of animal experiments described in this study were approved by the Institutional Animal care and Use committee at Cincinnati Children's Hospital Medical Center. *Fancc*$^{+/-}$ and *Fancd2*$^{+/-}$ mice were provided by Dr. Manuel Buchwald (Hospital for Sick Children, University of Toronto) and Dr. Markus Grompe (Oregon Health & Sciences University), respectively (8, 23). *Fancc* SKO, *Fancd2* SKO, and *Foxo3a* SKO mice were generated from interbreeding *Fancc*$^{+/-}$ or *Fancd2*$^{+/-}$ heterozygotes with the *Foxo3a*$^{+/-}$ mice (7), and WT and DKO mice were generated from interbreeding of the respective double heterozygotes. E13.5 embryos were harvested to compare the size of WT, SKO, and DKO embryos. MRI and CT were used to scan the brains of 2-month-old WT, SKO, and DKO mice as previously described (60). For mice on Quercetin diet, *Foxo3a*$^{+/-}$ *Fancd2*$^{+/-}$ breeders were supplied with Quercetin diet (10 mg/kg body weight per day; Harlan Laboratories).

RNA extraction and microarray analysis

Total RNA was isolated from the whole cerebrum of 2-month-old WT, SKO, and DKO mice, using the RNeasy Mini kit (Qiagen) according to the manufacturer's protocol. cRNA was synthesized from total RNA and hybridized to Affymetrix Mouse gene 1.0 ST array (Affymetrix, Inc.). The RNA quality and quantity assessment, probe preparation, labeling, hybridization, and image scan were carried out in the Cincinnati Children's Hospital Medical Center Affymetrix Core using standard procedures. Hybridization data were sequentially subjected to normalization, transformation, filtration, and functional classification. Data analysis was performed with Genespring GX11 (Agilent Technologies). Genes that were differentially expressed in SKO and DKO compared with WT mice brains with fold changes by 1.3 were analyzed by GSEA and Ingenuity Pathways Analysis (Ingenuity Systems). The enriched molecular signatures were considered overly represented with a *p*-value of ≤ 0.05.

FIG. 6. Increased DNA damage, apoptosis, and mitosis in DKO NSCs. (A) γ-H2AX staining of neurospheres formed by WT, *Foxo3a*$^{-/-}$ SKO, *Fancd2*$^{-/-}$ SKO, and *Foxo3a*$^{-/-}$ *Fancd2*$^{-/-}$ DKO NSCs. *Right panel*, quantification of cells with γ-H2AX foci ≥5 described in the *left panel* ($n = 5$). Scale bar represents 20 μm. **(B)** Flow cytometric analysis of apoptotic cells in the neurospheres formed by WT, *Foxo3a*$^{-/-}$ SKO, *Fancd2*$^{-/-}$ SKO, and *Foxo3a*$^{-/-}$ *Fancd2*$^{-/-}$ DKO NSCs. *Bottom panel*, quantification of Annexin V-positive cells ($n = 5$). **(C)** Cell-cycle analysis by BrdU incorporation of the NSCs in the neurospheres formed by WT, *Foxo3a*$^{-/-}$ SKO, *Fancd2*$^{-/-}$ SKO, and *Foxo3a*$^{-/-}$ *Fancd2*$^{-/-}$ DKO NSCs. *Bottom panels*, quantification of cells in the S and G2/M phases ($n = 5$). **(D)** pHH3 staining of E18.5 embryo brain sections of mice with the indicated genotypes. Original magnification, ×20. *Bottom panel*, quantification of dividing (pHH3-positive) cells on the ventricular surface of cortices in WT, SKO, and DKO brains at E18.5 ($n = 5$). *$p < 0.05$; **$p < 0.01$; and ***$p < 0.001$. pHH3, phospho-histone H3. To see this illustration in color, the reader is referred to the web version of this article at www.liebertpub.com/ars

Embryonic NPSCs isolation and neurosphere cultures

Telencephalons harvested from E12.5 days WT, SKO, and DKO embryos were dissociated into single cells by HyQTase cell detachment solution (Hyclone; Thermo Scientific) for 20 min at 37°C. The cells were washed and resuspended in culture medium [DMEM/F12 medium with 2% B27 supplement (Invitrogen), 50 μm N2 supplement (Invitrogen), 10 ng/ml EGF (R&D Systems), and 10 ng/ml FGF (R&D Systems)], triturated, filtered through a cell strainer (70 μm, BD Biosciences), counted by a hemocytometer, and plated at 4×10^3 cells/ml into multiwell ultra-low binding plates

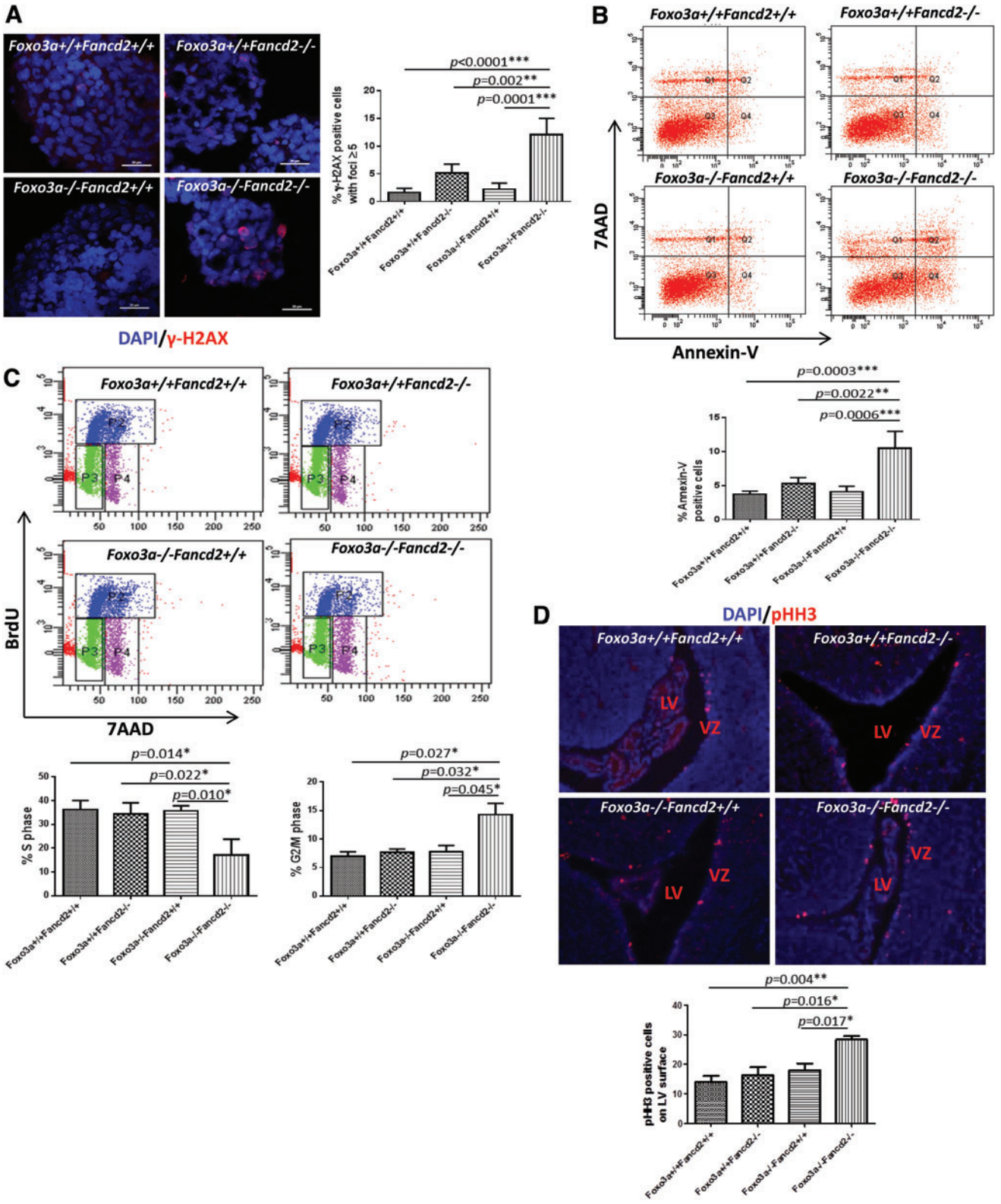

(Sigma). All cultures were maintained at 37°C in 5% CO_2/balance air.

To assess the self-renewal potential of cultured NSPCs, the size and number of primary neurospheres were detected, and the individual primary neurospheres were mechanically dissociated by trituration and then replated at clonal density into non-adherent cultures. Secondary neurospheres were counted 7 days later. Self-renewal is reported as the number of secondary neurospheres that arose per subcloned primary neurosphere.

For cell proliferation assays, dissociated embryonic NSCs were cultured for 6 days, then labeled with 10 μM BrdU for 24 h at 37°C. The neurospheres were dissociated to single-cell suspensions and cytospined to the slides before being fixed and stained with an antibody with BrdU.

To validate the role of ROS in NSC function, the freshly dissociated single NSCs were incubated with NAC (1 m*M*) for the entire culture period. The size and number of NAC-treated and -untreated neurospheres were measured at the 4th day after subcloning the primary neurosphere.

For the treatment of neurospheres with the Aurora B inhibitor Reversine, neuropsheres at passage 2 were dissociated into single cells and treated with Reversine (5 μM; Sigma) for 48 h. The neurosphere size and number were calculated 2 days later.

For transfection, neurospheres at passage 2 were dissociated into single cells, and then transfected with pcDNA5-BubR1 (47330; Addgene) and empty plasmid as control, using Lipofectamine 2000 (according to the manufacturer's guidelines; Invitrogen). The neurosphere size and number were measured 4 days later.

Intracellular ROS measurement

Primary neurospheres, adult brain cells, or SVZ area cells were dissociated into single-cell suspensions and then incubated with 2′-7′-dichlorofluorescein diacetate (DCF-DA) (25 μm; Sigma) for 30 min. DCF-DA is a cell-permeable non-fluorescent probe. It turns to highly fluorescent DCF on oxidation. The fluorescence intensity is proportional to the ROS levels within the cell cytosol. Propidium Iodide (PI) was used to stain the dead and dying cells. ROS production was only evaluated in living cells that are PI negative. Levels of fluorescent were measured by flow cytometry (BD Biosciences). The samples without DCF-DA treatment or PI staining were used as negative controls. Flowjo software was used to make the overlaid ROS flow graphs and calculate the mean of intensity.

BrdU incorporation and apoptosis detection

BrdU incorporation was performed on neurospheres using the BrdU Incorporation Kit (Roche) according to the manufacturer's protocol. The labeled neurospheres were dissociated into single-cell suspensions and analyzed by flow cytometry (BD Biosciences). Apoptosis of NSPCs was analyzed by flow cytometry (BD Biosciences) using the APC-conjugated annexin-V antibody and 7AAD.

Immunocytochemistry, histology, and immunohistochemistry

For immunocytochemistry on single-cell suspensions, cells were cytospined onto coverslips, fixed by 4% paraformaldehyde, permeabilized with blocking solution (1 × PBS/0.25% Trition X-100/5% BSA), and then processed for immunofluorescent detection with indicated primary and secondary antibodies (see the following antibodies were used). For immunocytochemistry on neurospheres, secondary neurospheres subcloned from primary neurosphere were cultured for 4 days, and collected for the immunofluorescent staining. The collected neurospheres were fixed with 4% paraformaldehyde overnight and cryoprotected with 30% sucrose in PBS at 4°C. For histology, cryosections (12 μm) were cut coronally with a Cryostat (Leica) and mounted onto superfrost-plus microscope slides (Fisher). Sections were stained with cresyl violet or H&E according to standard protocol. For immunostaining, coronal sections were washed with PBS and blocked with blocking solution (1 × PBS/0.25% Trition X-100/5% BSA). After overnight incubation with primary antibodies that were diluted in the blocking solution with gentle agitation at 4°C, sections were washed and incubated with appropriate Alexa-conjugated secondary antibodies (Alexa 488, 594, or 647, 1:200; Jackson ImmunoResearch). DNA was stained by using DAPI. For immunohistochemical staining, 12 μm frozen sections were first treated with 0.3% H_2O_2 for 20 min at RT to quench endogenous peroxidase activity, then blocked with blocking solution (10% donkey serum and 0.25% Triton X-100 in PBS), and labeled with primary antibody overnight at 4°C. Sections were washed and incubated with appropriate biotin-conjugated secondary antibodies for 2 h. Then, sections were treated with ABC solution (Vectastain ABC Elite Kit; Vector Laboratories) for 1 h, washed with PBS, and incubated with diaminobenzadine (DAB) substrate (Vector Laboratories) for 10 min. Images were collected on a Nikon C2 confocal microscope or a Zeiss Axivert 200 microscope, and multi-channel overlays were assembled in Image J.

The following primary antibodies were used: γ-H2AX (mouse, 1:200; Millipore), (rabbit, 1:400; Cell Signaling); Acetylate-α-tubulin (rabbit, 1:500; Sigma); Anti-pHH3 (rabbit, 1:400; Millipore), (rat, 1:200; Sigma); Tbr2 (rabbit, 1:400; Millipore); Active-caspase-3 (rabbit, 1:200; Cell Signaling); Foxp2 (rabbit, 1:500; Santa Cruz); Sox2 (rabbit, 1:300; Cell Signaling); Ki67 (rabbit, 1:400; Leica); BrdU (rat, 1:200; Abcam); and Cux1/2 (rabbit, 1:500; Santa Cruz).

FIG. 7. DKO NSCs display mitotic catastrophe. (A) Heat map of mitotic catastrophe-related genes in WT, SKO, and DKO brains. The expression levels of those genes are lower in DKO mice than in WT mice. **(B)** Primary neurospheres formed by the indicated NSCs were stained for γ-H2AX. Scale bar represents 50 μm. **(C)** Primary neurospheres formed by the indicated NSCs were stained for pHH3. Scale bar represents 50 μm. **(D)** Primary neurospheres formed by the indicated NSCs were stained for A-casp3. Scale bar represents 50 μm. **(E)** NSCs suspensions were stained for γ-H2AX, pHH3, A-casp3, and nuclear DNA. Cells simultaneously expressing γ-H2AX, pHH3, and A-casp3 are interpreted as mitotic catastrophe (indicated by *arrows*). Scale bar represents 50 μm. *Panels* with quantification are presented as mean ± SD from three independent experiments with $n = 5$ for each genotype. $^*p < 0.05$; $^{**}p < 0.01$. A-casp3, active-caspase-3. To see this illustration in color, the reader is referred to the web version of this article at www.liebertpub.com/ars

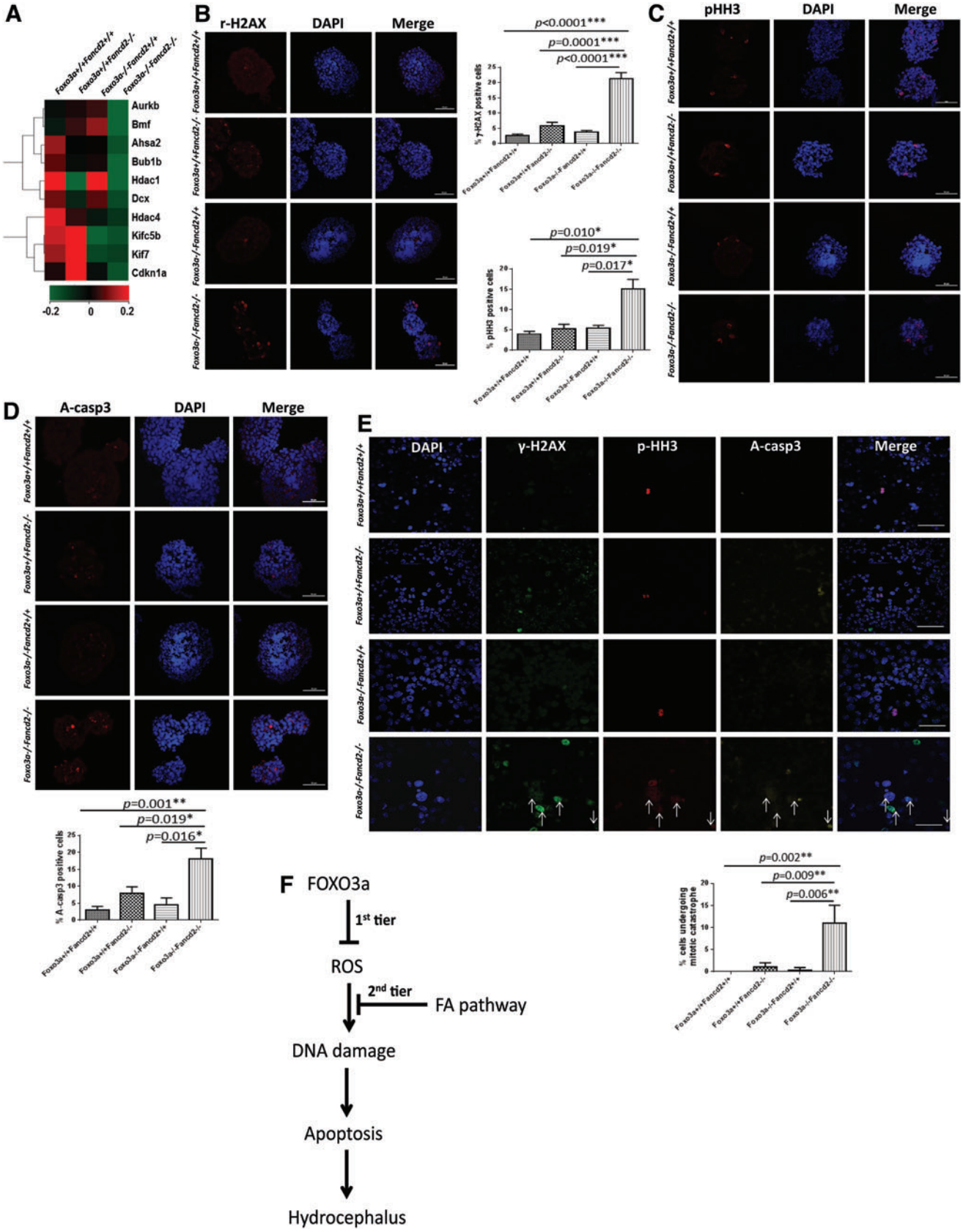
A
Foxo3a+/+Fancd2+/+
Foxo3a+/+Fancd2-/-
Foxo3a-/-Fancd2+/+
Foxo3a-/-Fancd2-/-
Aurkb
Bmf
Ahsa2
Bub1b
Hdac1
Dcx
Hdac4
Kifc5b
Kif7
Cdkn1a
-0.2
0
0.2
B
r-H2AX
DAPI
Merge
p<0.0001***
p=0.0001***
p<0.0001***
% γ-H2AX positive cells
p=0.010*
p=0.019*
p=0.017*
% pHH3 positive cells
C
pHH3
DAPI
Merge
D
A-casp3
DAPI
Merge
p=0.001**
p=0.019*
p=0.016*
% A-casp3 positive cells
E
DAPI
γ-H2AX
p-HH3
A-casp3
Merge
p=0.002**
p=0.009**
p=0.006**
% cells undergoing mitotic catastrophe
F
FOXO3a
1st tier
ROS
2nd tier
FA pathway
DNA damage
Apoptosis
Hydrocephalus

Quantitative real-time PCR

Total RNAs obtained from the 2-month-old brain tissues were reverse transcribed to cDNA by high-capacity cDNA reverse transcription kits (Applied Biosystems). Real-time PCR quantitative mRNA analyses were performed using SYBR green fluorescence (Qiagen). The primer sequences are provided in the Supplementary Table S2. The relative mRNA amount of each sample was calculated by fold change based on its threshold cycle, Ct, in comparison to the Ct of housekeeping gene Gapdh.

Statistics

Values are presented as mean ± SD. Statistical significance was determined using an unpaired Student's *t*-test. A *p*-value of < 0.05 was considered significant.

Acknowledgments

The authors thank Manuel Buchwald (Hospital for Sick Children, University of Toronto) for *Fancc*$^{+/-}$ mice; Markus Grompe (Oregon Health & Sciences University) for *Fancd2*$^{+/-}$ mice; Blaise Jones (Cincinnati Children's Hospital Medical Center) for critically reading this article; and Xiaona Liu, Mathieu Sertorio, and Diana Nardini for technical support. This work was supported by NIH grants R01 HL076712 and R01 CA157537. Q.P. is supported by a Leukemia and Lymphoma Scholar award.

Author Disclosure Statement

The authors declare no competing financial interests.

References

1. Bani-Yaghoub M, Tremblay RG, Lei JX, Zhang D, Zurakowski B, Sandhu JK, Smith B, Ribecco-Lutkiewicz M, Kennedy J, Walker PR, and Sikorska M. Role of Sox2 in the development of the mouse neocortex. *Dev Biol* 295: 52–66, 2006.
2. Banizs B, Pike MM, Millican CL, *et al.* Dysfunctional cilia lead to altered ependyma and choroid plexus function, and result in the formation of hydrocephalus. *Development* 132: 5329–5339, 2005.
3. Blalock EM, Geddes JW, Chen KC, Porter NM, Markesbery WR, and Landfield PW. Incipient Alzheimer's disease: microarray correlation analyses reveal major transcriptional and tumor suppressor responses. *Proc Natl Acad Sci U S A* 101: 2173–2178, 2004.
4. Brunet A, Sweeney LB, Sturgill JF, *et al.* Stress-dependent regulation of FOXO transcription factors by the SIRT1 deacetylase. *Science* 303: 2011–2015, 2004.
5. Caner H, Atasever A, Kilinc K, Durgun B, Peker S, and Ozcan OE. Lipid peroxide level increase in experimental hydrocephalus. *Acta Neurochir (Wien)* 121: 68–71, 1993.
6. Castillo P, Boqliolo M, and Surralles J. Coordinated action of the Fanconi anemia and ataxia telangiectasia pathways in response to oxidative damage. *DNA Repair (Amst)* 10: 518–525, 2011.
7. Castrillon DH, Miao L, Kollipara R, Horner JW, and DePinho RA. Suppression of ovarian follicle activation in mice by the transcription factor Foxo3a. *Science* 301: 215–218, 2003.
8. Chen M, Tomkins DJ, Auerbach W, *et al.* Inactivation of Fac in mice produces inducible chromosomal instability and reduced fertility reminiscent of Fanconi anaemia. *Nat Genet* 12: 448–451, 1996.
9. Cohen-Haguenauer O, Peault B, Bauche C, *et al. In vivo* repopulation ability of genetically corrected bone marrow cells from Fanconi anemia patients. *Proc Natl Acad Sci U S A* 103: 2340–2345, 2006.
10. Cong H, Jiang Y, and Tien P. Identification of the myelin oligodendrocyte glycoprotein as a cellular receptor for rubella virus. *J Virol* 85: 11038–11047, 2011.
11. Cumming RC, Lightfoot J, Beard K, Youssoufian H, O'Brien PJ, and Buchwald M. Fanconi anemia group C protein prevents apoptosis in hematopoietic cells through redox regulation of GSTP1. *Nat Med* 7: 814–820, 2001.
12. de Magalhaes JP, Curado J, and Church GM. Meta-analysis of age-related gene expression profiles identifies common signatures of aging. *Bioinformatics* 25: 875–881, 2009.
13. Du W, Adam Z, Rani R, Zhang X, and Pang Q. Oxidative stress in Fanconi anemia hematopoiesis and disease progression. *Antioxid Redox Signal* 10: 1909–1921, 2008.
14. Evans PH. Free radicals in brain metabolism and pathology. *Br Med Bull* 49: 577–587, 1993.
15. Ferland RJ, Cherry TJ, Preware PO, Morrisey EE, and Walsh CA. Characterization of Foxp2 and Foxp1 mRNA and protein in the developing and mature brain. *J Comp Neurol* 460: 266–279, 2003.
16. Fliegauf M, Benzing T, and Omran H. When cilia go bad: cilia defects and ciliopathies. *Nat Rev Mol Cell Biol* 8: 880–893, 2007.
17. Gong B, Cao Z, Zheng P, *et al.* Ubiquitin hydrolase Uch-L1 rescues beta-amyloid-induced decreases in synaptic function and contextual memory. *Cell* 126: 775–788, 2006.
18. Haberland M. Johnson A, Mokalled MH, Montgomery RL, and Olson EN. Genetic dissection of histone deacetylase requirement in tumor cells. *Proc Natl Acad Sci U S A* 106: 7751–7755, 2009.
19. He S, Iwashita T, Buchstaller J, Molofsky AV, Thomas D, and Morrison SJ. Bmi-1 over-expression in neural stem/progenitor cells increases proliferation and neurogenesis in culture but has little effect on these functions *in vivo. Dev Biol* 328: 257–272, 2009.
20. Ho GP, Margossian S, Taniquchi T, and D'Andrea AD. Phosphorylation of FANCD2 on two novel sites is required for mitomycin C resistance. *Mol Cell Biol* 26: 7005–7015, 2006.
21. Holden ST, Cox JJ, Kesterton I, Thomas NS, Carr C, and Woods CG. Fanconi anaemia complementation group B presenting as X linked VACTERL with hydrocephalus syndrome. *J Med Genet* 43: 750–754, 2006.
22. Homanics GE, Smith TJ, Zhang SH, Lee D, and Young SG. Targeted modification of the apolipoprotein B gene results in hypobetalipoproteinemia and developmental abnormalities in mice. *Proc Natl Acad Sci U S A* 90: 2389–2393, 1993.
23. Houghtaling S, Timmers C, Noll M, *et al.* Epithelial cancer in Fanconi anemia complementation group D2 (Fancd2) knockout mice. *Genes Dev* 17: 2021–2035, 2003.
24. Huang H and Tindall DJ. Dynamic FoxO transcription factors. *J Cell Sci* 120: 2479–2487, 2007.

25. Huh MS, Todd MA, and Picketts DJ. SCO-ping out the mechanisms underlying the etiology of hydrocephalus. *Physiology (Bethesda)* 24: 117–126, 2009.
26. Jiang H, Reinhardt HC, Bartkova J, Tommiska J, Blomqvist C, Nevanlinna H, Bartek J, Yaffe MB, and Hemann MT. The combined status of ATM and p53 link tumor development with therapeutic response. *Genes Dev* 23: 1895–1909, 2009.
27. Joenje H, Arwert F, Eriksson AW, de Koning H, and Oostra AB. Oxygen-dependence of chromosomal aberrations in Fanconi's anaemia. *Nature* 290: 142–143, 1981.
28. Kalsheker NA. Alpha 1-antichymotrypsin. *Int J Biochem Cell Biol* 28: 961–964, 1996.
29. Kennedy RD and D'Andrea AD. The Fanconi Anemia/BRCA pathway: new faces in the crowd. *Genes Dev* 19: 2925–2940, 2000.
30. Kim H and D'Andrea AD. Regulation of DNA cross-link repair by the Fanconi anemia/BRCA pathway. *Genes Dev* 26: 1393–1408, 2012.
31. Kopic S, Eirich K, Schuster B, *et al.* Hepatoblastoma in a 4-year-old girl with Fanconi anaemia. *Acta Paediatr* 100: 780–783, 2011.
32. Lee CK, Weindruch R, and Prolla TA. Gene-expression profile of the ageing brain in mice. *Nat Genet* 25: 294–297, 2000.
33. Lee SJ, Krauthauser C, Maduskuie V, Fawcett PT, Olson JM, and Rajasekaran SA. Curcumin-induced HDAC inhibition and attenuation of medulloblastoma growth *in vitro* and *in vivo*. *BMC Cancer* 11: 144, 2011.
34. Li J, Du W, Zhou Y, Maynard S, Andreassen PR, and Pang Q. Oxidative-stress specific interaction between FANCD2 and FOXO3a. *Blood* 115: 1545–1548, 2010.
35. McCauley J, Masand N, McGowan R, *et al.* X-linked VACTERL with hydrocephalus syndrome: further delineation of the phenotype caused by FANCB mutations. *Am J Med Genet A* 155A: 2370–2380, 2011.
36. Mootha VK, Lindgren CM, Eriksson KF, *et al.* PGC-1alpha-responsive genes involved in oxidative phosphorylation are coordinately downregulated in human diabetes. *Nat Genet* 34: 267–273, 2003.
37. Mori K, Miyake H, Kurisaka M, and Sakamoto T. Immunohistochemical localization of superoxide dismutase in congenital hydrocephalic rat brain. *Childs Nerv Syst* 9: 136–141, 1993.
38. Nadarajah B, Alifragis P, Wong RO, and Parnavelas JG. Neuronal migration in the developing cerebral cortex: observations based on real-time imaging. *Cereb Cortex* 13: 607–611, 2003.
39. Nieto M, Monuki ES, Tang H, *et al.* Expression of Cux-1 and Cux-2 in the subventricular zone and upper layers II-IV of the cerebral cortex. *J Comp Neurol* 479: 168–180, 2004.
40. Nuss JI, McCarl RL, Mulay IL, and Mulay LN. Copper and free radical accumulation in liver of calves with inherited hydrocephalus. *Am J Vet Res* 28: 1909–1913, 1967.
41. Paik JH, Ding Z, Narurkar R, *et al.* FoxOs cooperatively regulate diverse pathways governing neural stem cell homeostasis. *Cell Stem Cell* 5: 540–553, 2009.
42. Pece S, Tosoni D, Confalonieri S, *et al.* Biological and molecular heterogeneity of breast cancers correlates with their cancer stem cell content. *Cell* 140: 62–73, 2010.
43. Perez-Figares JM, Jimenez AJ, and Rodriguez EM. Subcommissural organ, cerebrospinal fluid circulation, and hydrocephalus. *Microsc Res Tech* 52: 591–607, 2001.
44. Qin S, Liu M, Niu W, and Zhang CL. Dysregulation of Kruppel-like factor 4 during brain development leads to hydrocephalus in mice. *Proc Natl Acad Sci U S A* 108: 21117–21121, 2011.
45. Renault VM, Rafalski VA, Morgan AA, *et al.* FoxO3 regulates neural stem cell homeostasis. *Cell Stem Cell* 5: 527–539, 2009.
46. Roninson IB, Broude EV, and Chang BD. If not apoptosis, then what? Treatment-induced senescence and mitotic catastrophe in tumor cells. *Drug Resist Updat* 4: 303–313, 2001.
47. Schmidt H, Siems WG, Grune T, and Grauel EL. Concentration of purine compounds in the cerebrospinal fluid of infants suffering from sepsis, convulsions and hydrocephalus. *J Perinat Med* 23: 167–174, 1995.
48. Sebastian JA Huang GJ, Cheung AF, *et al.* The T-box transcription factor eomes/tbr2 regulates neurogenesis in the cortical subventricular zone. *Genes Dev* 22: 2479–2484, 2008.
49. Sii-Felice K, Etienne O, Hoffschir F, *et al.* Fanconi DNA repair pathway is required for survival and long-term maintenance of neural progenitors. *EMBO J* 27: 770–781, 2008.
50. Soulier J. Fanconi anemia. Hematology Am Soc Hematol Educ Program 2011:492–497, 2011.
51. Spassky N, Merkle FT, Flames N, *et al.* Adult ependymal cells are postmitotic and are derived from radial glial cells during embryogenesis. *J Neurosci* 25: 10–18, 2005.
52. Svilar D, Goellner EM, Almeida KH, and Sobol RW. Base excision repair and lesion-dependent subpathways for repair of oxidative DNA damage. *Antioxid Redox Signal* 14: 2491–2507, 2011.
53. Tian Y, Lei L, and Minden A. A key role for Pak4 in proliferation and differentiation of neural progenitor cells. *Dev Biol* 353: 206–216, 2011.
54. Tothova Z, Kollipara R, Huntly BJ, *et al.* FoxOs are critical mediators of hematopoietic stem cell resistance to physiologic oxidative stress. *Cell* 128: 325–339, 2007.
55. Tsai WB, Chung YM, Takahashi Y, Xu Z, and Hu MC. Functional interaction between FOXO3a and ATM regulates DNA damage response. *Nat Cell Biol* 10: 460–467, 2008.
56. Turgut M, Erdogan S, Ergin K, and Serter M. Melatonin ameliorates blood-brain barrier permeability, glutathione, and nitric oxide levels in the choroid plexus of the infantile rats with kaolin-induced hydrocephalus. *Brain Res* 1175: 117–125, 2007.
57. Vitale I, Galluzzi L, Castedo M, and Kroemer G. Mitotic catastrophe: a mechanism for avoiding genomic instability. *Nat Rev Mol Cell Biol* 12: 385–392, 2011.
58. Vogel C, Hager C, and Bastians H. Mechanisms of mitotic cell death induced by chemotherapy-mediated G2 checkpoint abrogation. *Cancer Res* 67: 339–345, 2007.
59. Wong DJ, Liu H, Ridky TW, Cassarino D, Segal E, and Chang HY. Module map of stem cell genes guides creation of epithelial cancer stem cells. *Cell Stem Cell* 2: 333–344, 2008.
60. Wu J, Dombi E, Jousma E, *et al.* Preclincial testing of sorafenib and RAD001 in the Nf(flox/flox); DhhCre mouse model of plexiform neurofibroma using magnetic resonance imaging. *Pediatr Blood Cancer* 58: 173–180, 2012.

61. Yalcin S, Zhang X, Luciano JP, *et al.* Foxo3 is essential for the regulation of ataxia telangiectasia mutated and oxidative stress-mediated homeostasis of hematopoietic stem cells. *J Bio Chem* 283: 25692–25705, 2008.

Address correspondence to:
Dr. Qishen Pang
Division of Experimental Hematology
and Cancer Biology
Cincinnati Children's Hospital Medical Center
3333 Burnet Avenue
Cincinnati, OH 45229

E-mail: qishen.pang@cchmc.org

Date of first submission to ARS Central, August 20, 2013; date of final revised submission, January 21, 2014; date of acceptance, February 2, 2014.

Abbreviations Used

3V = third ventricle
A-casp3 = active-caspase-3
Ac-tubulin = acetylated α-tubulin
ATM = ataxia telangiectasia mutated
CSF = cerebrospinal fluid
CT = computerized tomography
Cx = cortex
DAB = diaminobenzadine
DCF-DA = 2′-7′-dichlorofluorescein diacetate
DKO = double knockout
FA = Fanconi anemia
FANCD2 = Fanconi anemia complementation group D2
FOXO = forkhead members of the class O
Hi = hippocampus
LV = lateral ventricle
MRI = magnetic resonance imaging
NAC = *N*-acetylcysteine
NSC = neural stem cell
NSPC = neural stem and progenitor cell
PCR = polymerase chain reaction
pHH3 = phospho-histone H3
PI = propidium lodide
ROS = reactive oxygen species
RT-qPCR = real-time quantitative polymerase chain reaction
SCO = subcommissural organ
SKO = single knockout
SOD = superoxide dismutases
SVZ = subventricular zone
VZ = ventricle zone
WT = wild type